

Probabilistic Gaussian Homotopy: A Probability-Space Continuation Framework for Nonconvex Optimization

Eshed Gal¹, Samy Wu Fung², and Eldad Haber¹

¹ University of British Columbia, Vancouver, BC, Canada

² Colorado School of Mines, Golden, CO, USA

Abstract. We introduce Probabilistic Gaussian Homotopy (PGH), a probability-space continuation framework for nonconvex optimization. Unlike classical Gaussian homotopy, which smooths the objective and uniformly averages gradients, PGH deforms the associated Boltzmann distribution and induces Boltzmann-weighted aggregation of perturbed gradients, which exponentially biases descent directions toward low-energy regions. We show that PGH corresponds to a log-sum-exp (soft-min) homotopy that smooths a nonconvex objective at scale $\lambda > 0$ and recovers the original objective as $\lambda \rightarrow 0$, yielding a posterior-mean generalization of the Moreau envelope, and we derive a dynamical system governing minimizer evolution along an annealed homotopy path. This establishes a principled connection between Gaussian continuation, Bayesian denoising, and diffusion-style smoothing. We further propose Probabilistic Gaussian Homotopy Optimization (PGHO), a practical stochastic algorithm based on Monte Carlo gradient estimation, and demonstrate strong performance on high-dimensional nonconvex benchmarks and sparse recovery problems where classical gradient methods and objective-space smoothing frequently fail.

Keywords: Homotopy · Global optimization · Gaussian smoothing · Moreau envelopes.

1 Introduction

Many problems in science and engineering can be formulated as the minimization of a highly nonconvex but differentiable objective

$$\min_{x \in \mathbb{R}^n} f(x), \quad (1)$$

where the landscape of f may contain numerous local minima, flat regions, and narrow basins of attraction. While local optimization methods are effective when initialized near a desirable solution, they often fail in strongly nonconvex settings. Global strategies such as simulated annealing [1], evolutionary methods [23], or multi-start schemes [21] attempt to address this challenge, but frequently suffer from slow convergence or poor scalability in high dimensions.

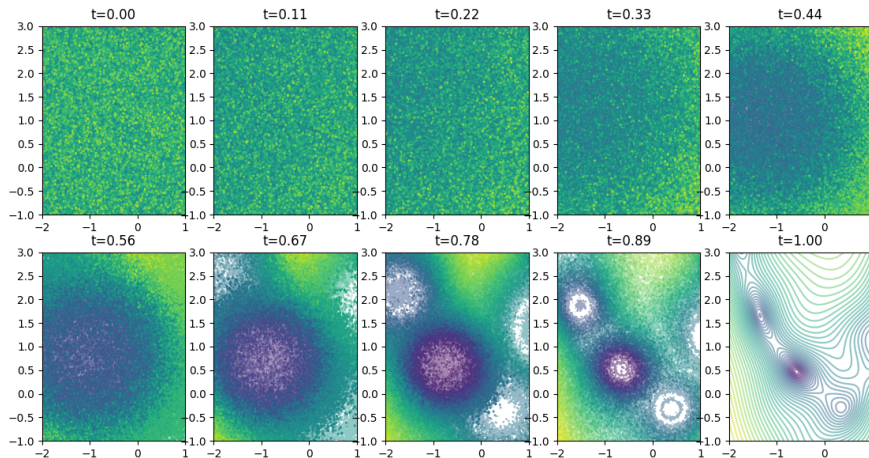


Fig. 1. Gaussian homotopy for the function $f(x_1, x_2) = \log(\text{Rosen}(x_1, x_2) + \alpha(1 + \sin(3x_1) \sin(3x_2)))$, where *Rosen* denotes the banana Rosenbrock function. We estimate the homotopy-smoothed objective by Monte Carlo sampling. The surface begins nearly flat and gradually deforms into a highly multimodal landscape that is much harder to optimize.

A classical approach for handling nonconvexity is *homotopy continuation* [11]. Rather than solving the difficult problem directly, one constructs a family of progressively less smoothed objectives and tracks minimizers as the smoothing is removed. Gaussian homotopy methods smooth the objective via convolution with a Gaussian kernel and gradually decrease the smoothing parameter [25,24]. Although effective in certain regimes, these methods operate in *objective space* and lack a direct connection to modern probabilistic modeling.

In parallel, score-based diffusion models have emerged as a powerful framework for high-dimensional generative modeling. These models define a family of progressively less noisy probability distributions and transport samples from a simple base density to a complex target distribution through a reverse-time stochastic differential equation. While primarily viewed as sampling algorithms, diffusion models implicitly define a *Gaussian homotopy in probability space*.

This observation motivates the central idea of this work. Minimizing an objective $f(x)$ is equivalent to maximizing its associated Boltzmann density

$$p(x) \propto \exp\left(-\frac{1}{\lambda}f(x)\right). \quad (2)$$

Instead of smoothing f directly, we smooth its induced probability distribution and track the evolution of high-probability regions as the smoothing vanishes. This yields a continuation method performed in *probability space*, fundamentally distinct from classical objective-space homotopy.

We formalize this idea through *Probabilistic Gaussian Homotopy (PGH)*, which constructs a time-dependent family of Gaussian-smoothed Boltzmann

densities via a soft-min (log-sum-exp) aggregation of perturbed objective values. As the smoothing decreases, the associated energy deforms continuously from a nearly flat landscape to the original nonconvex objective (see Figure 1). Minimizers are tracked along this path using a gradient-driven dynamical system.

The construction admits a natural Bayesian interpretation. Classical Moreau envelope smoothing corresponds to computing a Maximum A Posteriori (MAP) estimator under Gaussian perturbations. In contrast, PGH follows the posterior mean, which can be expressed via Tweedie’s formula [16,15] as a gradient of the log-marginal density. Replacing hard inner minimization with probabilistic averaging yields a tractable stochastic gradient estimator that aggregates information from a Gaussian neighborhood, biasing descent directions toward low-energy regions rather than relying solely on local curvature.

Contributions. Our contributions are summarized as follows.

- We reinterpret diffusion-style Gaussian smoothing as a homotopy mechanism for optimization, which establishes a bridge between classical Gaussian homotopy, Moreau envelope smoothing, and score-based diffusion.
- We introduce *Probabilistic Gaussian Homotopy (PGH)*, a probabilistic continuation framework that smooths the Boltzmann distribution associated with an objective rather than the objective itself.
- We establish a rigorous connection between this construction and Moreau envelope smoothing, showing that PGH corresponds to a posterior-mean (soft-min) variant of classical Moreau regularization.
- We derive an ordinary differential equation governing the evolution of minimizers along the homotopy and propose practical numerical schemes for tracking this path.

In summary, we introduce a principled probabilistic continuation framework that connects Bayesian denoising, diffusion dynamics, and global nonconvex optimization.

2 Background

We briefly review three fundamental concepts which underlies our framework: Gaussian homotopy in optimization, Moreau envelope smoothing, and score-based diffusion.

2.1 Gaussian Homotopy in Objective Space

Homotopy continuation methods address nonconvex optimization by embedding a difficult objective into a family of progressively less smoothed surrogates. Given $f : \mathbb{R}^n \rightarrow \mathbb{R}$, classical Gaussian homotopy constructs

$$F_\sigma(x) = (f * G_\sigma)(x) = \int_{\mathbb{R}^n} f(y) G_\sigma(x - y) dy, \quad (3)$$

where G_σ is a Gaussian kernel with variance σ^2 . Equivalently,

$$F_\sigma(x) = \mathbb{E}_{z \sim \mathcal{N}(0, I)}[f(x + \sigma z)]. \quad (4)$$

For large σ , F_σ is smooth and often easier to optimize; as $\sigma \rightarrow 0$, $F_\sigma \rightarrow f$.

The continuation strategy tracks minimizers $x^*(\sigma) \in \arg \min F_\sigma(x)$ while gradually decreasing σ . Gradients are given by

$$\nabla F_\sigma(x) = \mathbb{E}_z[\nabla f(x + \sigma z)], \quad (5)$$

so descent directions correspond to a uniform average of gradients in a Gaussian neighborhood.

While effective in certain regimes, this formulation operates directly in objective space and averages function values and gradients *uniformly*. As a result, competing basins contribute equally to the descent direction, which may potentially blur structural differences between low- and high-energy regions. This observation motivates exploring continuation directly in probability space rather than in objective space.

2.2 Moreau Envelope and Soft-Min Smoothing

Another classical smoothing construction is the Moreau envelope. For $\lambda > 0$, the Moreau envelope of f is defined as

$$M_\lambda f(x) = \min_y \left\{ f(y) + \frac{1}{2\lambda} \|x - y\|^2 \right\}. \quad (6)$$

The envelope replaces f by a locally regularized minimization problem. As $\lambda \rightarrow 0$, $M_\lambda f(x) \rightarrow f(x)$, while for larger λ the envelope becomes smoother and may reduce nonconvexity.

A useful probabilistic perspective arises from the soft-min (log-sum-exp) operator:

$$\text{softmin}_\lambda(g) = -\lambda \log \int \exp\left(-\frac{1}{\lambda} g(y)\right) dy. \quad (7)$$

By Laplace's principle, $\text{softmin}_\lambda(g)$ approximates $\min_y g(y)$ as $\lambda \rightarrow 0$. Applying this to

$$g(y) = f(y) + \frac{1}{2\lambda} \|x - y\|^2 \quad (8)$$

yields a smoothed approximation to the Moreau envelope that replaces hard minimization by probabilistic averaging. This observation provides a bridge between convexification methods and probabilistic smoothing.

2.3 Score-Based Diffusion and Gaussian Smoothing

Score-based diffusion models construct a family of probability densities $\{p_t\}_{t \in [0, 1]}$ by progressively adding Gaussian noise to data. A common forward noising process takes the form

$$x_t = \alpha(t)x_1 + \beta(t)\varepsilon, \quad \varepsilon \sim \mathcal{N}(0, I), \quad (9)$$

where $\beta(t)$ increases with t . Sampling is performed by integrating a reverse-time stochastic differential equation involving the score $\nabla_x \log p_t(x)$.

From a geometric viewpoint, diffusion defines a Gaussian homotopy in probability space: the density evolves continuously from a simple Gaussian to a complex target distribution. While diffusion models are typically interpreted as sampling algorithms, their structure naturally induces a continuation path across progressively de-smoothed distributions.

These three perspectives based on objective-space Gaussian homotopy, Moreau smoothing, and diffusion-based Gaussian perturbation, form the conceptual basis for the probabilistic homotopy framework developed in the next section.

3 Probabilistic Gaussian Homotopy

We now introduce *Probabilistic Gaussian Homotopy (PGH)*, a continuation framework that operates directly in probability space rather than in objective space. The key idea is to deform the Boltzmann density associated with f and track its minimizers as the smoothing vanishes.

3.1 Probability-Space Homotopy Construction

Let $f : \mathbb{R}^n \rightarrow \mathbb{R}$ be a possibly nonconvex objective and define its Boltzmann density

$$p_1(x) \propto \exp\left(-\frac{1}{\lambda(1)}f(x)\right). \quad (10)$$

Instead of smoothing f directly, we construct a time-dependent family of densities $\{p_t\}_{t \in [0,1]}$ by introducing Gaussian perturbations:

$$p_t(x) \propto \mathbb{E}_{z \sim \mathcal{N}(0,I)} \left[\exp\left(-\frac{1}{\lambda(t)}f(\alpha(t)x + \beta(t)z)\right) \right], \quad (11)$$

where $\alpha(t)$ and $\beta(t)$ define a smoothing schedule satisfying $\beta(1) = 0$ and $\beta(0) > 0$.

The corresponding energy functional is

$$F_t(x) = -\lambda(t) \log p_t(x). \quad (12)$$

This construction defines a continuous deformation of the objective landscape. At $t = 1$, $\beta(1) = 0$ and we recover the original objective,

$$F_1(x) = f(x). \quad (13)$$

At $t = 0$, strong smoothing renders $F_0(x)$ nearly constant, which yields a trivial optimization problem. Thus, $\{F_t\}$ forms a homotopy between a flat landscape and the original nonconvex objective, as observed in Figure 1. Crucially, smoothing occurs in the Boltzmann density rather than directly in f , producing a continuation mechanism fundamentally different from objective-space Gaussian homotopy.

3.2 Gradient Structure: Soft-Min Aggregation

To understand the geometry of this homotopy, we examine the gradient of F_t . Differentiating equation 12 yields

$$\nabla_x F_t(x) = \alpha(t) \frac{\mathbb{E}_z \left[\exp\left(-\frac{1}{\lambda(t)} f(\alpha(t)x + \beta(t)z)\right) \nabla f(\alpha(t)x + \beta(t)z) \right]}{\mathbb{E}_z \left[\exp\left(-\frac{1}{\lambda(t)} f(\alpha(t)x + \beta(t)z)\right) \right]}. \quad (14)$$

The gradient is therefore a *weighted average* of gradients in a Gaussian neighborhood of $\alpha(t)x$, where weights are proportional to $\exp(-f/\lambda)$. This induces a soft-min (log-sum-exp) aggregation. In particular, *perturbations with lower objective value contribute exponentially more to the descent direction*.

This contrasts with objective-space Gaussian homotopy, where gradients are averaged uniformly. Here, the continuation dynamics are biased toward low-energy regions, naturally emphasizing promising basins while suppressing high-energy perturbations.

3.3 Continuation Dynamics

Let

$$x^*(t) \in \arg \min_x F_t(x). \quad (15)$$

Under suitable regularity conditions, minimizers evolve smoothly with t . A natural mechanism for tracking this evolution is the non-autonomous gradient flow

$$\frac{dx(t)}{dt} = -\nabla_x F_t(x(t)). \quad (16)$$

Here, equation 16 defines a probability-space continuation dynamics. As t increases and smoothing decreases, trajectories follow the evolving minimizer path.

3.4 Stochastic Approximation and Discrete Scheme

In practice, expectations in equation 14 are approximated via Monte Carlo sampling. Given $z_k \sim \mathcal{N}(0, I)$,

$$\nabla_x F_t(x) \approx \alpha(t) \sum_{k=1}^K w_k(x, t) \nabla f(\alpha(t)x + \beta(t)z_k), \quad (17)$$

where

$$w_k(x, t) = \frac{\exp\left(-\frac{1}{\lambda(t)} f(\alpha(t)x + \beta(t)z_k)\right)}{\sum_j \exp\left(-\frac{1}{\lambda(t)} f(\alpha(t)x + \beta(t)z_j)\right)}. \quad (18)$$

This estimator replaces hard inner minimization with soft probabilistic aggregation and parallelizes naturally across samples.

Algorithm 1 Probabilistic Gaussian Homotopy Optimization (PGHO)

- 1: **Input:** Objective f , homotopy steps T , batch size B , samples K , step sizes $\{\eta_k\}$
- 2: Sample initial particles $x_i^0 \sim \mathcal{N}(0, I)$ for $i = 1, \dots, B$
- 3: **for** $k = 0$ to $T - 1$ **do**
- 4: $t_k \leftarrow k/(T - 1)$
- 5: **for** $i = 1$ to B **do**
- 6: Sample $z_{i,1}, \dots, z_{i,K} \sim \mathcal{N}(0, I)$
- 7: Compute Monte Carlo objective

$$F_{t_k}^{(K)}(x_i^k) = -\lambda(t) \log \left(\frac{1}{K} \sum_{j=1}^K \exp(-\lambda(t_k)^{-1} f(\alpha(t_k)x_i^k + \beta(t_k)z_{i,j})) \right) \quad (20)$$

- 8: Compute gradient
$$g_i^k = \nabla_x F_{t_k}^{(K)}(x_i^k) \quad (21)$$

- 9: Update
$$x_i^{k+1} \leftarrow x_i^k - \eta_k g_i^k \quad (22)$$

- 10: **end for**
 - 11: **end for**
 - 12: **Return** $\{x_i^T\}_{i=1}^B$
-

Discretizing equation 16 with time steps t_k yields

$$x_{k+1} = x_k - \eta_k \nabla_x F_{t_k}(x_k), \quad (19)$$

which simultaneously performs gradient descent on F_{t_k} and advances along the homotopy path. We refer to this procedure as *Probabilistic Gaussian Homotopy Optimization (PGHO)*. Multiple trajectories may be evolved in parallel, enabling exploration from diverse initializations. Algorithm 1 summarizes the procedure.

Computational Complexity. Each gradient evaluation requires K evaluations of f and ∇f , yielding total cost $\mathcal{O}(TBKC_f)$, where C_f denotes the cost of evaluating f and its gradient. All operations parallelize over batch and noise samples.

4 Connection to Moreau Envelopes and Bayesian Interpretation

We now show that Probabilistic Gaussian Homotopy (PGH) can be interpreted as a probabilistic, finite-temperature generalization of classical Moreau smoothing, and admits a natural Bayesian interpretation.

4.1 Soft Moreau Envelope

We now formalize the relationship between Probabilistic Gaussian Homotopy (PGH) and a finite-temperature (log-sum-exp) relaxation of the Moreau envelope.

Recall that the Moreau envelope of f with parameter $\lambda > 0$ is defined as

$$M_\lambda f(x) = \min_y \left\{ f(y) + \frac{1}{2\lambda} \|x - y\|^2 \right\}. \quad (23)$$

Replacing the hard minimum in equation 23 by a soft-min (log-sum-exp) operator yields the finite-temperature surrogate

$$\widetilde{M}_\lambda f(x) = -\lambda \log \int \exp \left(-\frac{1}{\lambda} \left(f(y) + \frac{1}{2\lambda} \|x - y\|^2 \right) \right) dy. \quad (24)$$

We now show that PGH coincides with this soft Moreau envelope under a particular parameter choice.

Theorem 1 (PGH as Soft Moreau Envelope). *Let $F_t(x)$ denote the PGH energy defined in equation 12. If $\alpha(t) = 1$ and $\beta(t) = \sqrt{\lambda(t)}$, then*

$$F_t(x) = \widetilde{M}_{\lambda(t)} f(x) + C(t), \quad (25)$$

where $C(t)$ is a constant independent of x .

Proof. Starting from equation 24, perform the change of variables

$$y = x + \sqrt{\lambda}z, \quad dy = \lambda^{n/2} dz. \quad (26)$$

Then $\|x - y\|^2 = \lambda \|z\|^2$, and equation 24 becomes

$$\widetilde{M}_\lambda f(x) = -\lambda \log \int \exp \left(-\frac{1}{\lambda} f(x + \sqrt{\lambda}z) \right) \exp \left(-\frac{1}{2} \|z\|^2 \right) dz + C, \quad (27)$$

where C absorbs normalization constants independent of x . Recognizing the Gaussian density yields

$$\widetilde{M}_\lambda f(x) = -\lambda \log \mathbb{E}_{z \sim \mathcal{N}(0, I)} \left[\exp \left(-\frac{1}{\lambda} f(x + \sqrt{\lambda}z) \right) \right] + C. \quad (28)$$

This matches the PGH energy with $\alpha = 1$ and $\beta = \sqrt{\lambda}$. \square

The theorem shows that PGH reduces to a finite-temperature (soft) Moreau envelope under the canonical scaling $\beta^2 = \lambda$. Thus, PGH can be interpreted as a probabilistic relaxation of classical Moreau smoothing in which hard minimization is replaced by Gaussian-weighted averaging.

4.2 Bayesian Interpretation and Posterior Mean Dynamics

Similarly, we formalize the Bayesian interpretation of PGH and show that its gradient dynamics correspond to posterior-mean updates under Gaussian perturbations.

Consider the denoising model

$$x = y + \sqrt{\lambda}z, \quad z \sim \mathcal{N}(0, I), \quad (29)$$

with Gibbs prior

$$\pi(y) \propto \exp(-f(y)). \quad (30)$$

The posterior distribution of y given x is

$$p(y | x) \propto \exp\left(-f(y) - \frac{1}{2\lambda}\|x - y\|^2\right). \quad (31)$$

The Maximum A Posteriori (MAP) estimator of equation 31 coincides with the Moreau minimizer equation 23. In contrast, PGH follows the posterior mean.

Theorem 2 (Posterior Mean Identity). *Define the marginal density*

$$p_\lambda(x) = \int \exp(-f(y)) \mathcal{N}(x; y, \lambda I) dy, \quad (32)$$

and the associated probabilistic envelope

$$F_\lambda(x) = -\log p_\lambda(x). \quad (33)$$

Then the posterior mean satisfies

$$\mathbb{E}[y | x] = x - \lambda \nabla F_\lambda(x). \quad (34)$$

Proof. Differentiating $p_\lambda(x)$ under the integral sign yields

$$\nabla_x p_\lambda(x) = \int \exp(-f(y)) \nabla_x \mathcal{N}(x; y, \lambda I) dy. \quad (35)$$

Using the Gaussian score identity

$$\nabla_x \mathcal{N}(x; y, \lambda I) = -\frac{1}{\lambda}(x - y) \mathcal{N}(x; y, \lambda I), \quad (36)$$

we obtain

$$\nabla_x \log p_\lambda(x) = -\frac{1}{\lambda}(x - \mathbb{E}[y | x]). \quad (37)$$

Rearranging yields equation 34. \square

This theorem shows that gradient descent on the probabilistic envelope F_λ corresponds exactly to a posterior-mean update:

$$x \leftarrow x - \eta \nabla F_\lambda(x) \iff x \leftarrow (1 - \eta)x + \eta \mathbb{E}[y | x]. \quad (38)$$

Thus, PGH replaces the MAP-based hard minimization of the Moreau envelope by posterior-mean dynamics driven by Gaussian perturbations. This finite-temperature update remains well-defined even in highly nonconvex regimes, where MAP estimators may be unstable or difficult to compute. PGH can therefore be interpreted as a posterior-mean generalization of Moreau smoothing.

5 Related Work

Gaussian Homotopy in Optimization. Gaussian homotopy (GH) methods have a long history in global optimization, often leveraging heat-equation-based smoothing to regularize nonconvex landscapes [11,25]. Classical GH constructs a family of smoothed objectives $F(x, t) = (f * G_{\sigma(t)})(x)$ by convolving the objective function f with a Gaussian kernel [25]. Continuation is achieved by gradually reducing the smoothing parameter while tracking minimizers. More recent variants, such as Single-Loop GH (SLGH) [14], improve computational efficiency by updating the smoothing parameter and optimization variables simultaneously. Despite these advances, existing GH methods operate strictly in *objective space*, which average function values and gradients uniformly across perturbations [25,24]. In contrast, our approach performs continuation in *probability space*, which smoothens the induced Boltzmann distribution $p(x) \propto \exp(-\frac{1}{\lambda}f(x))$ rather than the raw objective. This shift fundamentally alters the geometry of the descent direction, introducing a soft-min aggregation mechanism absent in classical GH.

Score-Based Diffusion Models. Score-based diffusion models have recently achieved remarkable success in high-dimensional generative modeling by learning to reverse a forward Gaussian noising process [37,8]. These methods construct a continuum of intermediate densities and sample by integrating a reverse-time stochastic differential equation driven by the score function $\nabla_x \log p_t(x)$. While diffusion models are primarily studied in the context of sampling and image generation, their structure naturally defines a Gaussian homotopy in probability space. Connections between diffusion and inverse problems have begun to emerge, but the interpretation of diffusion dynamics as a principled continuation method for *global optimization* remains largely unexplored. Our work makes this connection explicit by showing that probability-space smoothing induces a minimizer path analogous to classical homotopy methods.

Moreau Envelopes and Bayesian Estimation. The Moreau envelope is a central tool in convex analysis and proximal algorithms [13,30,28,2,10,9], providing a smooth regularization of nonsmooth or nonconvex objectives. It has recently been applied in large-scale and federated optimization settings [33,13,30,22]. From a statistical viewpoint, the envelope corresponds to a Maximum A Posteriori (MAP) estimator under Gaussian perturbations [34]. Recent work has further developed log-integral (log-sum-exp) approximations to infimal convolutions via Laplace’s method [36,6,7], which replaces hard minimization with finite-temperature exponential averaging and yields a posterior-mean interpretation. PGH aligns with this probabilistic perspective. In particular, it can be viewed as a finite-temperature, Boltzmann-weighted generalization of Moreau smoothing. However, rather than approximating proximal maps, we use this log-integral structure to define a continuation path in probability space and derive dynamics that track minimizers as smoothing vanishes. This connects Laplace-based smoothing, Bayesian denoising, and diffusion-based homotopy within a unified framework.

Stochastic Gradient Estimation and Graduated Optimization. Our stochastic gradient estimator builds on classical results for gradient estimation of expectations [16,5]. Unlike standard stochastic gradient descent, which evaluates ∇f at a single point, PGH computes a weighted average of gradients over a Gaussian neighborhood. This mechanism shares similarities with entropy-regularized methods [4], but differs in that the weights are derived from the Boltzmann energy, which emphasizes low-energy perturbations exponentially. As a result, the continuation dynamics selectively amplify promising descent directions rather than uniformly averaging local curvature.

Global optimization algorithms. Random-search methods, such as Pure Random Search (PRS) [3], sample points from the domain and keep the best value observed. Population-based heuristics such as Differential Evolution (DE) [31] and Particle Swarm Optimization [18] maintain a set of candidate solutions and update them using randomized recombination or velocity-style rules, respectively. Basin Hopping (BH) [38,29] combines random perturbations with local refinement steps, accepting or rejecting moves based on the resulting objective value. Annealing-based methods [20] allow occasional uphill moves with a temperature-controlled probability, enabling escape from local minima. Implicit Filtering (IF) [17] is a derivative-free local method based on stencil sampling with a sequence of decreasing step sizes, and is often used for noisy or non-smooth objectives. Finally, the Covariance Matrix Adaptation Evolution Strategy (CMA-ES) [12] adapts a Gaussian search distribution by learning its covariance over time, yielding efficient search directions on ill-conditioned landscapes. In contrast to these black-box global optimization heuristics, our method exploits gradient information and performs a continuation procedure through a probabilistic smoothing of the induced Boltzmann distribution, producing a Boltzmann-weighted aggregation of perturbed gradients. This yields a structured descent direction that remains stable in highly multimodal landscapes.

6 Numerical Experiments

6.1 Benchmark Problems

To evaluate the capability of our method to converge on challenging non-convex objectives, we consider standard benchmark functions: Ackley, Griewank, Alpine1, and Levy, taken from the Virtual Library of Simulation Experiments [32]. Figure 2 visualizes representative of those functions in the 2D case, and shows representative convergence trajectories from several random initializations.

We next compare our method with a series of global optimization algorithms, including classical Gaussian Homotopy (GH), Covariance Matrix Adaptation Evolution Strategy (CMA-ES) [12], Differential Evolution (Diff.Eval.) [31], Basin Hopping (BasinHop.) [38,29], (Simulated / Dual) Annealing (Anneal.) [20], Implicit Filtering (Impl.Filt.) [17], Particle Swarm (Part.Swarm) [18], and Pure Random Search (PRS) [3]. We also report two variants of our approach: *PGH-GD* and *PGH-Adam*, which share the same probabilistic homotopy objective but differ

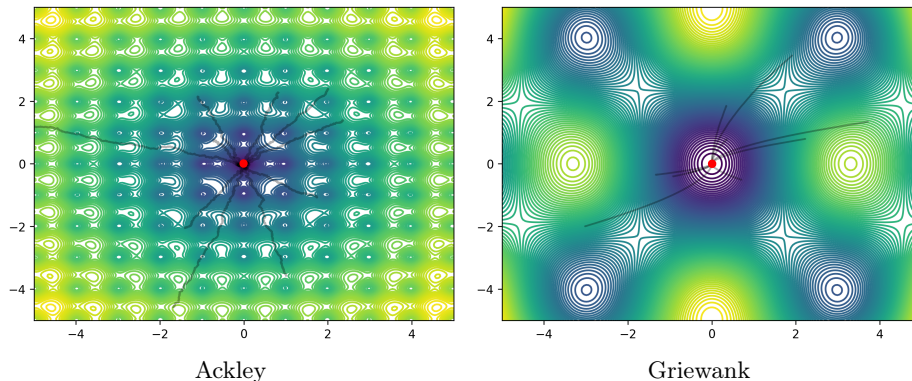


Fig. 2. Ackley and Griewank plotted for the 2D case with the trajectories obtained by the PGH algorithms starting from different points

Table 1. Mean number of function evaluations required to reach success (“N” indicates no successful runs), where success is defined as $f(x) < 5 \times 10^{-2}$. Each run uses a maximum budget of 2×10^5 function evaluations. Results are averaged over 30 runs at dimension $n = 10$.

Function	PGH-GD	PGH-Adam	GH	CMAES	Diff.Eval.	BasinHop.	Anneal.	Impl.Filt.	Part.Swarm	PRS
Ackley	205	601	3,894	804	6,683	N	97,646	240	3,663	N
Griewank	183	631	3,248	1,088	8,937	14,120	99,785	315	4,891	N
Alpine1	192	557	3,479	1,176	11,367	N	97,195	308	4,187	N
Levy	3,067	562	3,141	817	5,731	N	85,933	N	3,146	N

only in the base update rule used for the inner step (gradient descent vs. Adam [19]). Table 1 summarizes the results. Overall, our method is the fastest across these benchmarks, consistently reaching the target tolerance with substantially fewer evaluations than the competing baselines.

We further report convergence behavior and scalability on these benchmarks. Figure 3 reports success rate as a function of dimension, where our method remains highly consistent even as the dimension increases, while some competing methods degrade substantially in higher dimensions. This highlights that the probabilistic aggregation in our method provides a stable search direction in settings where other global optimizers may struggle to scale. Additional convergence results and experimental details for the are provided in the appendix.

6.2 Sparse Recovery

We next consider sparse recovery from undersampled linear measurements, which provides a standard and challenging nonconvex inverse problem. We observe

$$y = Ax^* + \eta, \quad (39)$$

where $A \in \mathbb{R}^{m \times n}$ is a sensing matrix with $m < n$, $x^* \in \mathbb{R}^n$ is a sparse ground-truth signal, and η is additive noise. Our goal is to recover x^* from y by solving a sparsity-promoting regression problem.

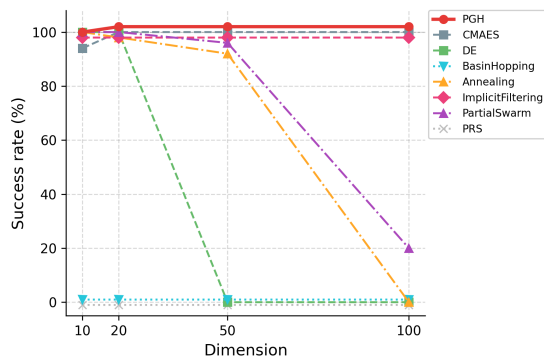


Fig. 3. Success rate vs. dimension on Ackley. PGH maintains high success rate across all dimensions, while competing methods degrade significantly on higher dimensions. Budget fixed at 10^5 function evaluations, averaged over 30 runs.

In particular, we study the ℓ_0 -regularized least-squares formulation

$$\min_{x \in \mathbb{R}^n} \frac{1}{2} \|Ax - y\|_2^2 + \lambda \|x\|_0, \quad (40)$$

which balances data fidelity with sparsity of the recovered signal [27]. While there are many possible relaxations for this problem [35,26], in this work we focus on a smooth approximation to the ℓ_0 regularization.

$$f_\tau(x) = \frac{1}{2} \|Ax - y\|_2^2 + \lambda \sum_{i=1}^n \left(1 - e^{-x_i^2/\tau^2}\right), \quad (41)$$

where $\tau > 0$ controls the sharpness of the approximation. As $\tau \rightarrow 0$, the penalty approaches the counting function $\|x\|_0$, while for fixed τ it remains differentiable and can be handled by gradient-based methods.

We compare two variants of our method, *PGH-GD* and *PGH-Adam*, against the corresponding baseline optimizers *GD* and *Adam*. We evaluate the methods along a regularization path over λ and focus on the main qualitative outcomes. *Note that we do not compare different ℓ_0 relaxations but rather the use of different optimization algorithms to solve this particular relaxation.* Additional implementation details are provided in the Appendix.

Figure 4 summarizes the sparse recovery results. Figure 4(a) shows the tradeoff between the data misfit $\frac{1}{2} \|Ax - y\|_2^2$ and the smooth ℓ_0 term $\sum_i (1 - e^{-x_i^2/\tau^2})$. This plot plays the role of an L-curve: better solutions lie closer to the lower-left region, where one achieves both low reconstruction error and stronger sparsity. The PGH-based methods trace a more favorable frontier than the baseline methods over most of the path, indicating an improved sparsity–fidelity tradeoff.

Figure 4(b) shows the attained objective value $f_\tau(x)$ as a function of λ . Both PGH variants obtain lower objective values than standard GD and Adam. The

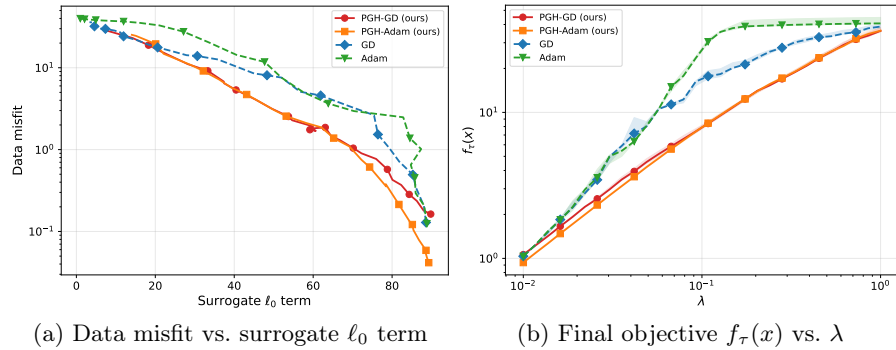


Fig. 4. Sparse recovery results along the regularization path. Left: tradeoff between reconstruction fidelity and sparsity. Right: attained smooth objective value as a function of the regularization parameter. In both plots, the PGH variants improve over the corresponding GD and Adam baselines.

improvement is particularly visible in the intermediate range of λ , where the balance between fitting the measurements and enforcing sparsity is most delicate. This suggests that the probabilistic homotopy mechanism helps the optimizer navigate the nonconvex landscape more effectively and avoid poorer local minima.

Overall, these experiments indicate that our methods provide a consistent improvement over the corresponding first-order baselines for sparse recovery. Empirically, PGH leads to solutions that are both more competitive in objective value and better balanced in terms of sparsity and data fidelity.

7 Conclusion

In this work, we introduced Probabilistic Gaussian Homotopy (PGH), a continuation framework that operates in probability space rather than directly in objective space, leading to Boltzmann-weighted aggregation of perturbed gradients that emphasizes low-energy regions and provides a principled search direction for difficult nonconvex problems. We further established connections to finite-temperature Moreau-type smoothing and a posterior-mean interpretation, and demonstrated across a range of nonconvex optimization settings that PGH yields strong empirical performance, including favorable results on benchmark test problems and improved behavior on sparse recovery. Overall, these results suggest that probability-space continuation is a promising and effective alternative to classical smoothing approaches for challenging nonconvex optimization.

Disclosure of Interests. The authors have no competing interests to declare that are relevant to the content of this article.

References

1. Bertsimas, D., Tsitsiklis, J.: Simulated annealing. *Statistical science* **8**(1), 10–15 (1993)
2. Boyd, S., Vandenberghe, L.: *Convex optimization*. Cambridge University press (2004)
3. Brooks, S.H.: A discussion of random methods for seeking maxima. *Operations Research* **6**(2), 244–251 (1958)
4. Chaudhari, P., Choromanska, A., Soatto, S., LeCun, Y., Baldassi, C., Borgs, C., Chayes, J., Sagun, L., Zecchina, R.: Entropy-sgd: Biasing gradient descent into wide valleys. *Journal of Statistical Mechanics: Theory and Experiment* **2019**(12), 124018 (2019)
5. Dalalyan, A.S.: Theoretical guarantees for approximate sampling from smooth and log-concave densities. *Journal of the Royal Statistical Society: Series B (Statistical Methodology)* **79**(3), 651–676 (2017)
6. Darbon, J., Langlois, G.P.: On bayesian posterior mean estimators in imaging sciences and hamilton–jacobi partial differential equations. *Journal of Mathematical Imaging and Vision* **63**(7), 821–854 (2021)
7. Darbon, J., Langlois, G.P., Meng, T.: Connecting hamilton-jacobi partial differential equations with maximum a posteriori and posterior mean estimators for some non-convex priors. In: *Handbook of Mathematical Models and Algorithms in Computer Vision and Imaging: Mathematical Imaging and Vision*, pp. 1–25. Springer (2021)
8. Dhariwal, P., Nichol, A.: Diffusion models beat gans on image synthesis. *Advances in Neural Information Processing Systems* **34**, 8780–8794 (2021)
9. Di, N., Chi, E.C., Fung, S.W.: A monte carlo approach for nonsmooth convex optimization via proximal splitting algorithms. *arXiv preprint arXiv:2509.07914* (2025)
10. Di, N., Chi, E.C., Fung, S.W.: Operator splitting with hamilton-jacobi-based proximals. *arXiv preprint arXiv:2601.22370* (2026)
11. Dunlavy, D.M., O’Leary, D.P.: *Homotopy optimization methods for global optimization*. Tech. rep., Sandia National Laboratories (SNL) (2005)
12. Hansen, N., Ostermeier, A.: Completely derandomized self-adaptation in evolution strategies. *Evolutionary Computation* **9**(2), 159–195 (2001)
13. Heaton, H., Wu Fung, S., Osher, S.: Global solutions to nonconvex problems by evolution of hamilton-jacobi pdes. *Communications on Applied Mathematics and Computation* **6**(2), 790–810 (2024)
14. Iwakiri, H., Wang, Y., Ito, S., Takeda, A.: Single loop gaussian homotopy method for non-convex optimization. In: *Advances in Neural Information Processing Systems*. vol. 35, pp. 7065–7076 (2022)
15. Kailath, T.: The innovations approach to detection and estimation theory. *Proceedings of the IEEE* **58**(5), 680–695 (1970)
16. Kaipio, J., Somersalo, E.: *Statistical and computational inverse problems*, vol. 160. Springer Science & Business Media (2006)
17. Kelley, C.T.: *Implicit Filtering*. Society for Industrial and Applied Mathematics (SIAM), Philadelphia, PA (2011)

18. Kennedy, J., Eberhart, R.: Particle swarm optimization. In: Proceedings of the IEEE International Conference on Neural Networks. pp. 1942–1948. IEEE, Perth, Australia (1995)
19. Kingma, D.P., Ba, J.: Adam: A method for stochastic optimization. In: International Conference on Learning Representations (ICLR) (2015)
20. Kirkpatrick, S., Gelatt, C.D., Vecchi, M.P.: Optimization by simulated annealing. *Science* **220**(4598), 671–680 (1983)
21. Martí, R., Resende, M.G., Ribeiro, C.C.: Multi-start methods for combinatorial optimization. *European Journal of Operational Research* **226**(1), 1–8 (2013)
22. Meng, T., Liu, S., Fung, S.W., Osher, S.: Recent advances in numerical solutions for hamilton-jacobi pdes. arXiv preprint arXiv:2502.20833 (2025)
23. Michalewicz, Z.: Heuristic methods for evolutionary computation techniques. *Journal of Heuristics* **1**(2), 177–206 (1996)
24. Mobahi, H., Fisher III, J.W.: On the link between gaussian homotopy continuation and convex envelopes. In: International Workshop on Energy Minimization Methods in Computer Vision and Pattern Recognition. pp. 43–56. Springer (2015)
25. Mobahi, H., Fisher III, J.W.: A theoretical analysis of optimization by gaussian continuation. In: Proceedings of the AAAI Conference on Artificial Intelligence. vol. 29 (2015)
26. Mohimani, H., Babaie-Zadeh, M., Jutten, C.: A fast approach for overcomplete sparse decomposition based on smoothed ℓ_0 norm. *IEEE Transactions on Signal Processing* **57**(1), 289–301 (2009). <https://doi.org/10.1109/TSP.2008.2007606>
27. Natarajan, B.K.: Sparse approximate solutions to linear systems. *SIAM Journal on Computing* **24**(2), 227–234 (1995)
28. Nocedal, J., Wright, S.: Numerical optimization. Springer (1999)
29. Olson, B.S., Hashmi, I., Molloy, K., Shehu, A.: Basin hopping as a general and versatile optimization framework for the characterization of biological macromolecules. *Advances in Artificial Intelligence* **2012**, 674832:1–674832:19 (2012)
30. Osher, S., Heaton, H., Wu Fung, S.: A hamilton–jacobi-based proximal operator. Proceedings of the National Academy of Sciences **120**(14), e2220469120 (2023)
31. Storn, R., Price, K.: Differential evolution—a simple and efficient heuristic for global optimization over continuous spaces. *Journal of Global Optimization* **11**(4), 341–359 (1997)
32. Surjanovic, S., Bingham, D.: Virtual library of simulation experiments: Test functions and datasets. <http://www.sfu.ca/~ssurjano> (2013), retrieved June 23, 2021
33. T Dinh, C., Tran, N., Nguyen, J.: Personalized federated learning with moreau envelopes. *Advances in neural information processing systems* **33**, 21394–21405 (2020)
34. Tenorio, L.: Statistical regularization of inverse problems. *SIAM Review* **43**, 347–366 (2001)
35. Tibshirani, R.: Regression shrinkage and selection via the lasso. *Journal of the Royal Statistical Society: Series B (Methodological)* **58**(1), 267–288 (1996). <https://doi.org/10.1111/j.2517-6161.1996.tb02080.x>
36. Tibshirani, R.J., Fung, S.W., Heaton, H., Osher, S.: Laplace meets moreau: Smooth approximation to infimal convolutions using laplace’s method. *Journal of Machine Learning Research* **26**(72), 1–36 (2025)
37. Vincent, P.: A connection between score matching and denoising autoencoders. *Neural Computation* **23**(7), 1661–1674 (2011)
38. Wales, D.J., Doye, J.P.K.: Global optimization by basin-hopping and the lowest energy structures of Lennard-Jones clusters containing up to 110 atoms. *The Journal of Physical Chemistry A* **101**(28), 5111–5116 (1997)

A Additional Convergence Results

To further illustrate the behavior of the proposed method, Figure 5 reports convergence curves for PGH-Adam on four representative benchmark functions in dimension 10. For each problem, we plot the median best objective value over 20 runs together with the interquartile range. The curves show that PGH-Adam makes steady progress across several nonconvex landscapes, while the spread across runs remains reasonably controlled. These additional results complement the aggregate performance measures in the main text by showing the optimization dynamics more directly.

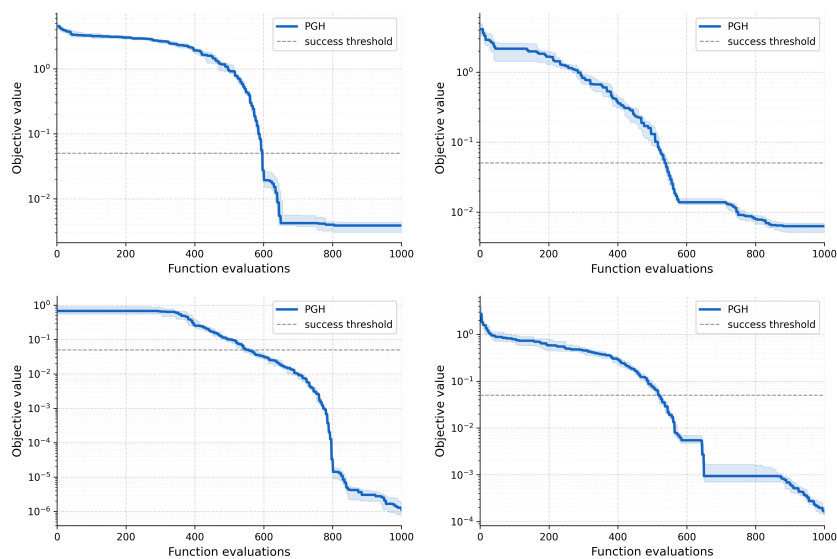


Fig. 5. Convergence of PGH-Adam on four benchmark functions ($d = 10$). Solid line shows the median best objective value over 20 runs; shaded region shows the interquartile range; dashed line marks the success threshold (5×10^{-2}).

B Experimental Details

B.1 Benchmark Problems

We evaluate the method on four standard nonconvex benchmark functions: Ackley, Griewank, Alpine1, and Levy. Unless otherwise stated, experiments are run in dimension $n = 10$, with a maximum budget of 2×10^5 function evaluations and 30 independent random trials. Success is defined by the threshold $f(x) < 5 \times 10^{-2}$. All methods are initialized from a random point sampled uniformly from the standard box constraints of the corresponding benchmark function, as stated

in [32]. Specifically, we use the domains $[-5, 5]^n$ for Ackley, $[-600, 600]^n$ for Griewank, and $[-10, 10]^n$ for Alpine1 and Levy. All methods are evaluated under the same function-evaluation budget and the same success criterion as in the main text. Results are reported as the mean number of function evaluations required to reach the target threshold, with “N” indicating that no successful run was observed within the allotted budget.

Benchmark Objective Functions. We evaluate the method on four standard nonconvex benchmark functions.

Ackley function.

$$f_{\text{Ackley}}(x) = -20 \exp \left(-0.2 \sqrt{\frac{1}{n} \sum_{i=1}^n x_i^2} \right) - \exp \left(\frac{1}{n} \sum_{i=1}^n \cos(2\pi x_i) \right) + 20 + e. \quad (42)$$

Griewank function.

$$f_{\text{Griewank}}(x) = \frac{1}{40} \sum_{i=1}^n x_i^2 - \prod_{i=1}^n \cos \left(\frac{x_i}{\sqrt{i}} \right) + 1. \quad (43)$$

Alpine1 function.

$$f_{\text{Alpine1}}(x) = \sum_{i=1}^n |x_i \sin(x_i) + 0.1x_i|. \quad (44)$$

Levy function.

$$f_{\text{Levy}}(x) = \sin^2(\pi w_1) + \sum_{i=1}^{n-1} (w_i - 1)^2 (1 + 10 \sin^2(\pi w_i + 1)) + (w_n - 1)^2 (1 + \sin^2(2\pi w_n)). \quad (45)$$

where

$$w_i = 1 + \frac{x_i - 1}{4}, \quad i = 1, \dots, n. \quad (46)$$

The global minimizers are $x^* = 0$ for Ackley, Griewank, and Alpine1, and $x^* = (1, \dots, 1)$ for Levy.

PGH Variants and Hyperparameters. We report two variants of our method, *PGH-GD* and *PGH-Adam*, which share the same probabilistic homotopy objective and differ only in the base optimizer used in the update step. In both cases, the PGH gradient is estimated by Monte Carlo sampling with antithetic perturbation pairs. All PGH runs use $K = 4$ Monte Carlo samples per step; the only exception is PGH-GD on Levy, where we use $K = 16$ to reduce variance. The homotopy parameter is increased from 0 to 1 over a prescribed number of homotopy steps, after which the method continues at full homotopy until the evaluation budget is exhausted. Across the benchmark problems, the number of homotopy steps was tuned per problem and typically ranged from 50 to 200. Both PGH-GD and PGH-Adam use cosine learning-rate schedules over the homotopy phase, so the tuned values are interpreted as initial learning rates. These initial learning rates were also selected separately for each problem and optimizer, and ranged approximately from 10^{-1} to 5×10^1 , reflecting differences in scaling and landscape geometry across the benchmark functions. In all cases, the iterates are constrained to remain within the benchmark search box.

B.2 Sparse Recovery

For the sparse recovery experiments, we consider signals of ambient dimension $n = 10,000$ with sparsity level $k = 100$, observed through undersampled linear measurements with sampling ratio $m/n = 0.15$ and additive Gaussian noise of standard deviation $\sigma = 0.01$. The smooth ℓ_0 parameter is set to $\tau = 0.05$, and results are averaged over 3 independent trials. We sweep the regularization parameter over a log-spaced grid with $\lambda \in [10^{-2}, 1]$ using 30 values.

For the PGH methods, we use $K = 4$ Monte Carlo samples per iteration, with a maximum of 10,000 iterations, corresponding to a total budget of 4×10^4 function evaluations. PGH uses learning rate 0.05. We use perturbation scale $\varepsilon = 0.1$ and minimum homotopy parameter $t_{\min} = 0.37$. The homotopy parameter is updated using a square-root schedule, so that it increases gradually from t_{\min} to 1 over the course of the run. We choose $t_{\min} > 0$ to avoid the near-zero homotopy regime, where gradients become very small and optimization can progress slowly. In the PGH implementation, antithetic perturbation pairs are used in the Monte Carlo gradient estimate to reduce variance. For the baseline methods, GD uses learning rate 0.05 and Adam uses learning rate 0.01 for stability. All methods use cosine annealing schedules, and are initialized from the zero vector.